



# Continuous Preparation of Chitosan-Based Self-Powered Sensing Fibers Recycled from Wasted Materials for Smart Home Applications

Yingying Li<sup>1,2</sup> · Chuanhui Wei<sup>1,3</sup> · Yang Jiang<sup>1,3</sup> · Renwei Cheng<sup>1,3</sup> · Yihan Zhang<sup>1,3</sup> · Chuan Ning<sup>1,3</sup> · Kai Dong<sup>1,3</sup> · Zhong Lin Wang<sup>1,3,4</sup>

Received: 1 June 2022 / Accepted: 15 August 2022

© Donghua University, Shanghai, China 2022

## Abstract

Currently, the gradual depletion of fossil resources and the large amount of plastic waste are causing serious harm to the land and marine ecology. The rapid development of wearable smart fibers is accompanied by rapid growth in the material demand for fibers, and the development of green and high-performance biomass-based fibers has become an important research topic to reduce the dependence on synthetic fiber materials and the harm to the environment. Here, chitosan is first prepared from the waste material by chemical methods. Then the chitosan-based self-powered induction fibers are prepared by electrospinning core wire technique. Chitosan-based self-powered sensing fiber is ultra-light and flexible, which can achieve about 2500 collisions without damaging the surface. Chitosan-based self-powered sensing fiber can also be used in smart home sensing applications to control home appliance switches with a light touch, which has a great application prospect in smart home and wearable fields.

**Keywords** Recycled wasted materials · Chitosan nanofibers · Electrospinning · Self-powered sensing · Smart home

## Introduction

Textiles are one of the basic necessities of people's daily life [1]. With the continuous development of human civilization, people's lifestyles have undergone great changes [2]. Textiles are also not just warm and decorative but appear in daily life as smart wearable electronic products [3, 4]. Fibers have

also changed from natural fibers and man-made synthetic fibers to conductive fibers and smart fibers [5]. Smart fibers are flexible, lightweight and comfortable, and can be integrated into textiles as sensors for detecting breathing [6, 7], sleep [8], movement [9, 10], medical rehabilitation [11], etc. However, in the case of wearable devices, their continuous operation needs to solve the problem of frequent charging and battery replacement [12]. Triboelectric nanogenerators (TENGs), which combine the effects of contact electricity and electrostatic induction, generate electricity from various mechanical stimuli, such as friction, vibration, rotation, and expansion/contraction motions [13–15]. Textile-based TENGs have been developed by combining TENGs and traditional textiles [16, 17]. With both energy harvesting and self-powered sensing functions, it provides an effective strategy for powering wearable devices [18]. It has broad application prospects in wearable micro/nano power supply [19], self-powered sensing [2], health monitoring [7], bionic system [20], human–machine interface [21], artificial intelligence [22], etc.

The choice of materials for TENGs is very wide [23–25], and most of the materials used in the current experiments are metals or polymer materials, which are not only very expensive but also not easily degradable that can cause serious

✉ Kai Dong  
dongkai@binn.cas.cn

✉ Zhong Lin Wang  
zhong.wang@mse.gatech.edu

<sup>1</sup> CAS Center for Excellence in Nanoscience, Beijing Key Laboratory of Micro-Nano Energy and Sensor, Beijing Institute of Nanoenergy and Nanosystems, Chinese Academy of Sciences, Beijing 101400, People's Republic of China

<sup>2</sup> Center On Nanoenergy Research, School of Physical Science and Technology, Guangxi University, Nanning 530004, People's Republic of China

<sup>3</sup> School of Nanoscience and Technology, University of Chinese Academy of Sciences, Beijing 100049, People's Republic of China

<sup>4</sup> School of Material Science and Engineering, Georgia Institute of Technology, Atlanta, GA 30332-0245, USA

pollution to the environment [26]. The earth is currently experiencing a serious environmental and energy crisis, and the increasing amount of waste plastics and depleting energy sources are the main challenges to be faced [27]. Therefore, it is necessary to find recyclable and inexpensive green materials. Chitin is the second largest natural polymer after cellulose, which is mainly found in the exoskeletons of insects and crustaceans, in the cell membranes of algal organisms and in the cell walls of plants [28, 29]. Chitosan is the product of chitin deacetylation, which has high chemical reactivity, excellent antibacterial activity, biocompatibility and biodegradability, and has broad application prospects in agriculture, medicine, food, cosmetics, environmental protection, etc. [30, 31]. As a green, environmentally friendly, and natural material, chitosan has also received wide attention in the application of TENGs, such as the preparation of biodegradable and breathable electronic skin [32], motion sensing and power supply of electronic devices [33], humidity sensors to detect physiological signals [34], etc. However, research on the use of chitosan for wearable sensing fibers is still relatively scarce.

Here, chitosan-based self-powered sensing fibers are prepared, where chitosan is obtained from waste materials, such as shrimp shells. Chitin is first extracted from the waste shrimp shells and then deacetylated to obtain chitosan. Chitosan is further prepared into nanofibers, and then chitosan nanofibers are tightly wrapped on silver-plated nylon yarn by electrospinning core-yarn technique to prepare chitosan-based self-powered sensing fibers. The strength and softness of chitosan-based self-powered sensing fibers can be adjusted by swapping different central conductive yarns. In addition, chitosan-based self-powered sensing fibers can be used to control smart home appliances (such as desk lamps, fans, monitors, humidifiers, etc.), which have great potential applications in smart home sensing.

## Experimental Section

### Chemicals and Materials

All laboratory grade chemicals and solvents were used without further purification, whereas all electrospinning experiments were carried out at room temperature. The conductive material uses commercial silver-coated nylon yarn which is non-toxic, non-hazardous, stable in performance and not easy to wear. Shrimp shells were purchased from Taobao.com. Sodium hydroxide (NaOH) (> 97%, SigmaAldrich), hydrochloric acid (HCl) (36–38%, Xi Hua), ethanol (> 99.7%, Yong Da Chemical), acetone (> 99.5%, Xi Hua) and deionized water (DI) were used to treat the shrimp shells. Dichloromethane (DCM) (> 99.5%, Yong Da Chemical) and trifluoroacetic acid (TFA) (> 99%, Macklin) were used to configure the spinning solution.

### Process of Chitosan Extraction from Wasted Materials

Choose to recover chitosan from discarded shrimp shells. Place the shrimp shells in a clean beaker and added deionized water. The beaker was then placed in an ultrasonic cleaner for initial cleaning of the shrimp shells (20 min per ultrasonic cleaning, 4 washes), which was filtered at the end of the cleaning and the shrimp shells were dried in an oven at 60 °C. The dried shrimp shells were placed in a 0.25 M hydrochloric acid solution and the calcium carbonate impurities were removed by constant stirring with a glass rod at room temperature (repeated several times). The shrimp shells were soaked in hydrochloric acid solution overnight, and then hydrochloric acid was added dropwise to the solution, and no bubbles were produced by stirring, which indicated that the reaction was saturated. The shrimp shells were filtered and washed several times with deionized water to neutral and dried in an oven at 60 °C. Afterwards, the shrimp shells were placed in a 1 mol/L sodium hydroxide solution with the aim of removing the proteins (heated at 70 °C and the process was repeated until the solution was colorless). The shrimp shells were filtered, rinsed several times with deionized water to neutrality and dried in an oven at 60 °C. Next, the shrimp shells were boiled in acetone to remove the remaining impurities. The shrimp shells were cleaned using hot alcohol and then rinsed with deionized water to neutral and dried in an oven at 60 °C. At this point, chitin was obtained. Finally, chitin was converted to chitosan by deacetylation reaction. Chitin was placed in 45 wt% sodium hydroxide solution (80 °C, 12 h), filtered, washed with deionized water to neutral, and dried in an oven at 60 °C (the process was repeated twice) to obtain chitosan. The degree of deacetylation of the resulting chitosan was 92.1%.

### Preparation of Chitosan Electrospinning Solution

In the present work, various concentrations of chitosan were electrospun using different processing parameters. The concentration of chitosan was 1.5, 2, 2.5% (w/w) and the ratio of solvent TFA/DCM was 90/10, 80/20, 70/30, 60/40, 50/50% (v/v), respectively. It was stirred at room temperature until completely dissolved and left to stand overnight to expel air bubbles. The structural morphology and diameters of electrospun nanofibers were determined on a SEM.

### Preparation of Chitosan-Based Self-Powered Sensing Fibers

First, the prepared solution was loaded into two different 5 mL plastic syringes fitted with 21 G metal nozzles and fixed in a homemade rotating device. Secondly, these two metal nozzles were connected to a positive and negative

power supply. There was a certain distance from the nozzles to the edge of the metal funnel, and the positive and negative voltage of the chitosan spinning solution was set to  $\pm 9$  kV. The chitosan solution was fed at a rate of 1 mL/h. During the spinning process, the spinneret jets were ejected from the electrodes due to their opposite charges and were attracted to each other above the metal funnel to form a spinning triangle. Through the rotating funnel collector, the nanofibers in the spinning triangle were wound on the silver-plated nylon yarn to obtain chitosan-based self-powered sensing fibers. The prepared chitosan-based self-powered sensing fiber was collected using the reel device for continuous production.

## Characterization and Measurement

To characterize the electrical output performance of the chitosan-based self-powered sensing fibers, a linear motor was used to provide periodic contact-separation motion. The contact length was 50 mm, the tapping force was 10 N, and the maximum motion distance was set to 20 mm. The surface morphology of the chitosan-based self-powered sensing fibers, the stages of the shrimp shell treatment process, and the cross-section of the chitosan-based self-powered sensing fibers were characterized by field emission scanning electron microscopy (Nova Nano SEM 450), respectively. XRD (Xper3 power) was used to characterize the crystalline structure of chitin and chitosan. FT-IR (VERTEX80v, Brucker) spectrometer was used to measure the infrared spectra of chitin and chitosan. Thermogravimetric analysis of chitin and chitosan was performed in the range of 30–600 °C at a rate of 10 °C min<sup>-1</sup> in an argon atmosphere (TG, Mettler Toledo). Stress-strain tests of chitosan-based self-powered sensing fibers were performed using a Labthink/XLM-50 N system. To measure the electrical output capability of the chitosan-based self-powered sensing fibers, an external force was applied with a commercial linear mechanical motor. The applied force was detected by a compression dynamometer (Vernier LabQuest Mini).  $V_{OC}$ ,  $I_{SC}$  and  $Q_{SC}$  were measured by a Keithley 6541 electrometer.

## Results and Discussions

Chitosan is a green and natural material that can be obtained from the bones or shells of animals. Here, waste shrimp shells are selected as the original material to extract chitosan, and chitosan-based self-powered sensing fibers are prepared by electrospun core-yarn technology to realize sensing control applications for household appliances, as shown in Fig. 1a. Figure 1b shows the flow chart of chitosan extraction from shrimp shells. Chitosan is obtained by deacetylation of chitin. Chitin is a biopolymer similar to cellulose and is the main component of the shell of many lower

animals, especially arthropods (e.g. insects, crustaceans, etc.), mainly in the form of inorganic salts (mainly calcium carbonate) and protein-bound. The shrimp shells are first ultrasonically cleaned with deionized water to remove surface stains. Then the cleaned shrimp shells are put into dilute hydrochloric acid solution for decalcification to remove impurities such as calcium carbonate from the shrimp shells. After the removal of calcium impurities, shrimp shells into dilute alkaline solution are heated and stirred to remove impurities such as proteins. Then the shrimp shells stripped of calcium impurities and proteins are heated in acetone to remove the remaining organic impurities. Finally, the treated shrimp shells are filtered and rinsed to neutral and dried in an oven to obtain chitin. The extracted chitin is put into 45 wt% sodium hydroxide solution and heated and stirred to carry out the chemical reaction of deacetylation to obtain chitosan.

Figure S1 (Supporting Information) shows physical diagram of the various processes used to recover chitosan from shrimp shells. The impurity content of shrimp shells before treatment is very high and gray, as shown in Fig. S1a. After the decalcification process, the surface color of shrimp shells changes to orange-yellow and the surface of shrimp shells is smoother, as shown in Fig. S1b. After the removal of calcium impurities, proteins and other impurities, the surface color of shrimp shells is white at this time, as shown in Fig. S1c. After the deacetylation reaction, the surface color of the shrimp shell is light yellow, as shown in Fig. S1d. To more directly understand the changes in shrimp shells during the extraction of chitosan, the microscopic surface morphology is also observed by scanning electron microscopy (SEM), as shown in Fig. 1c. As shown in Fig. 1c(i), the surface of the untreated shrimp shells is very rough and covered with various granular calcareous impurities. After the decalcification reaction as shown in Fig. 1c(ii), there are no more granular impurities on its surface, but there are flaky impurities attached to its surface. After further reaction of removing protein and other impurities, it can be seen that there are many more small pores evenly arranged on its surface, and there are no other impurities on its surface as shown in Fig. 1c(iii). After the deacetylation reaction of shrimp shells in sodium hydroxide solution, as shown in Fig. 1c(iv), the pores on the surface of shrimp shells disappeared and small cracks appeared.

The chitin deacetylation to chitosan in the shrimp shell extraction experiment is analyzed by X-ray diffraction (XRD), Fourier transform infrared spectroscopy (FT-IR) and thermogravimetry (TG). As Fig. 1d shows the XRD of chitin and chitosan extracted from shrimp shells, and the inset shows the XRD of untreated shrimp shells. It can be seen that there are many spurious peaks in the XRD patterns of the untreated shrimp shells, which disappeared after the chitin extraction experiment (For example, the diffraction

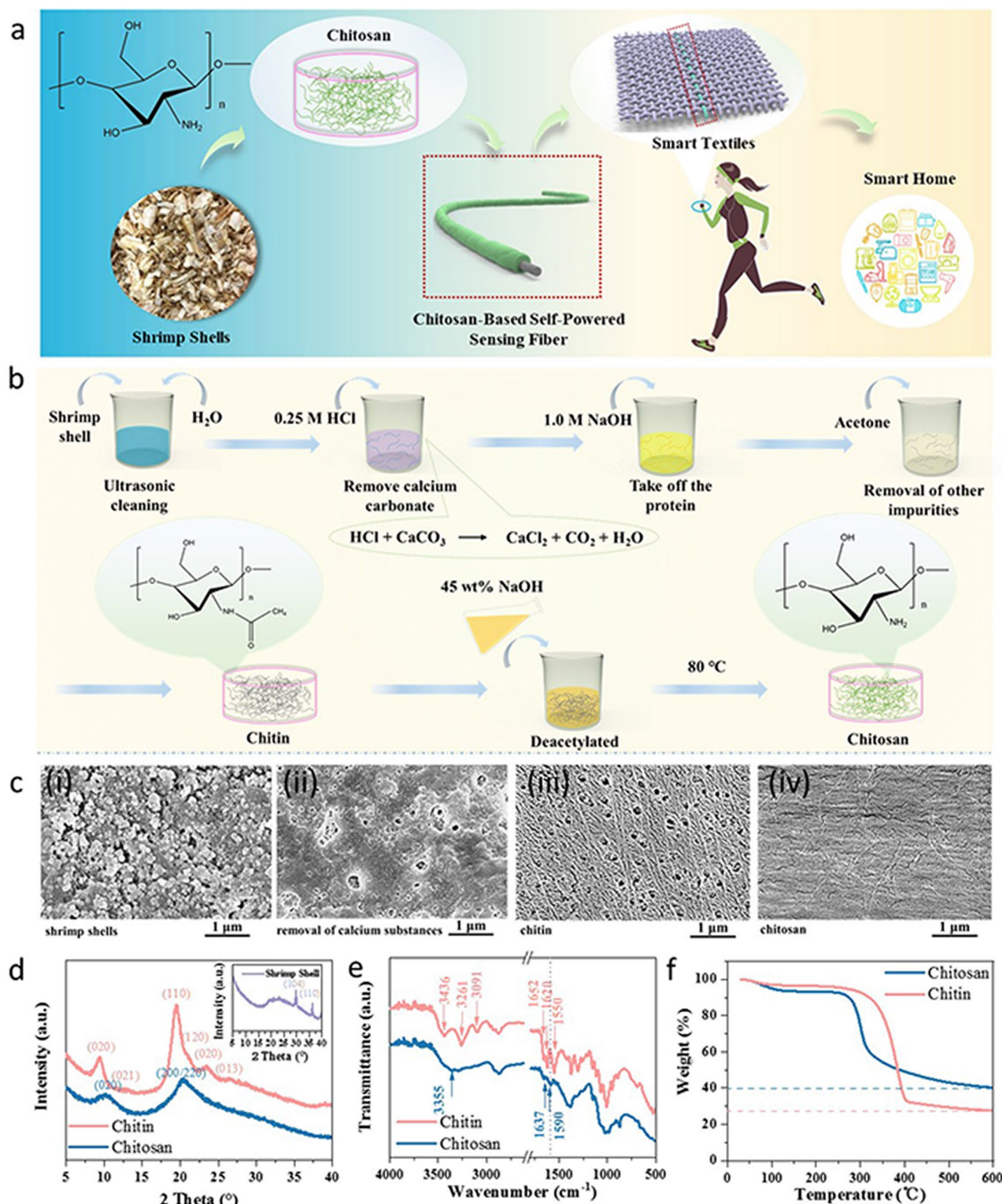


**Fig. 1** Process and performance characterization of chitosan recycled from waste materials. **a** Chitosan recycled from shrimp shells as sensing in smart home. **b** Flow chart of chitosan recovery from shrimp shells. **c** SEM charts in different stages. (i) Untreated shrimp shells. (ii) Shrimp shells after removal of calcium substances. (iii) Chitin. (iv) Chitosan. **d** XRD patterns of chitosan and chitin. The inset shows the XRD image of the untreated shrimp shell. **e** FT-IR spectra of chitosan and chitin. **f** TG curves of chitosan and chitin

peaks at 29.9° and 36.2°, respectively (104) (110)). The XRD curves of chitin have diffraction peaks at  $\theta=9.4^\circ$ , 12.8°, 19.5°, 20.9°, 23.4° and 26.4°, corresponding to the (020), (021), (110), (120) and (013) reflections of  $\alpha$ -chitin, respectively. Chitosan shows two characteristic diffraction peaks at about 10.1° and 20°, corresponding to the (020) reflection and the superimposed peak (200)/(220) reflection of chitosan crystals, respectively [27]. It indicates that the chitin treated with sodium hydroxide solution undergo a deacetylation reaction and was converted to chitosan. Figure 1e shows the FT-IR spectra of chitin and chitosan extracted from shrimp shells. The FT-IR spectra of chitin show the characteristic absorption peaks at  $3436\text{ cm}^{-1}$ ,  $3261\text{ cm}^{-1}$  and  $3091\text{ cm}^{-1}$  (OH and N–H stretching),  $1652\text{ cm}^{-1}$  and  $1620\text{ cm}^{-1}$  for the amide I band ( $\nu(\text{C=O})$ ) and  $1550\text{ cm}^{-1}$  for the amide II band ( $\delta(\text{N–H})$ ) [24]. After treatment of chitin with sodium hydroxide solution, the peaks corresponding to  $3436\text{ cm}^{-1}$  and  $3261\text{ cm}^{-1}$  merged to  $3355\text{ cm}^{-1}$ , the peak corresponding to  $1620\text{ cm}^{-1}$  in the bimodal amide I band merged with the stretching peak at  $1652\text{ cm}^{-1}$  to  $1637\text{ cm}^{-1}$ , and the peak corresponding to the amide II band red-shifted from  $1550$  to  $1590\text{ cm}^{-1}$ . This indicates the conversion of chitin to chitosan by deacetylation reaction. Figure 1f shows the TG analysis of chitin and chitosan extracted from shrimp shells. The maximum thermal decomposition temperature of chitin is about 285 °C and the residual rate of the sample mass at 600 °C is 27.5%. The maximum thermal decomposition temperature of chitosan is about 251 °C, and the residual rate of sample mass at 600 °C is 40%. The thermal decomposition temperature of chitosan is lower than that of chitin, but the residual mass of chitosan is higher than that of chitin at the end of the experiment [27]. This is mainly due to the presence of amide groups in chitin, so its thermal stability is higher. These results confirm the conversion of chitin to chitosan by deacetylation reaction in sodium hydroxide solution.

As shown in Fig. 2a(i), electrospinning equipment that can be continuous and automated is used to fabricate chitosan-based self-powered sensing fiber. The spinning solvent for chitosan is a mixture of solvents (trifluoroacetic acid: dichloromethane (TFA: DCM)), as shown in Fig. 2a(ii). The configured solvent mixes are 9:1, 8:2, 7:3, 6:4 and 5:5 (v: v) for TFA: DCM, respectively [35–37]. Weigh a certain amount of chitosan and put it into the well-mixed solvent to configure 2 wt% chitosan solution. Inject the chitosan spinning solution into the syringe and put it into the propulsion pump of the electrospinning device to prepare chitosan-based self-powered sensing fibers. The electrospinning equipment consists of a funnel collector and two symmetrical electrospinning systems. During the spinning process, conductive fibers are first passed through the funnel and then wound by a winding device placed on the opposite side of the funnel. Then, two symmetrical electrospinning

devices start spinning the chitosan spinning solution, and chitosan nanofibers are deposited onto the spinning funnel to form a nanofiber network covering the end of the funnel. During continuous winding of the conductive core wire, the nanofiber web is pulled, twisted and constrained into nanofiber bundles that completely cover the conductive core wire. The chitosan nanofibers are uniformly wound around the conductive yarn at an angle to form a spiral fiber bundle, which is a tightly wrapped core–shell structure. First, the effects of different solvent ratios on chitosan nanofibers are briefly discussed. For the preparation of 2 wt% chitosan nanofibers, the solvent ratios are TFA: DCM = 9:1, 8:2 and 7:3, respectively, as shown in Fig. S2. It can be observed that when TFA: DCM = 9:1 and 8:2, the chitosan filaments have very many bead-like links and poor morphology. When TFA: DCM = 7:3, the spun chitosan filaments have very few bead-like structures, but some linkages are present and the morphology has changed better. When the TFA: DCM is 6:4 and 5:5, the mixed solvent cannot completely dissolve the chitosan and will precipitate in the solvent in layers, as shown in Fig. S3, so these two cases are not discussed for the time being. In summary, a solvent with TFA: DCM ratio of 7:3 is chosen to prepare chitosan spinning solution.

Figure 2b shows the spool diagram of the prepared chitosan-based self-powered sensing fibers, and Fig. 2c shows the physical photo of the spool of chitosan-based self-powered sensing fibers. The chitosan-based self-powered sensing fiber is shown in Fig. 2d(i) as a core–shell structure, with chitosan nanofibers in green and silver-plated nylon yarn in gray. SEM images of the surface morphology of chitosan-based self-powered sensing fibers, as shown in Fig. 2d(ii). The fineness of the chitosan-based self-powered sensing fiber is very small, only about 350  $\mu\text{m}$  in diameter. The cross-sectional morphology is shown in Fig. 2d(iii), where the chitosan nanofibers are tightly wrapped around the silver-plated nylon yarn. The mechanical strength and fineness of the chitosan-based self-powered sensing fibers are two key points to demonstrate the quality of the fibers, such as deformability, weight, flexibility and comfort. The chitosan-based self-powered sensing fibers are fabricated by spirally wrapping chitosan nanofibers around the conductive yarn on the support of silver-plated nylon yarn. Thus, the softness of the whole chitosan-based self-powered sensing fibers depends on the conductive yarn and the dielectric material. Silver-plated nylon yarn, which has the same flexibility as ordinary yarn, was chosen as the material for the chitosan-based self-powered sensing fibers in this work. Chitosan-based self-powered sensing fibers have characteristics such as ultra-lightweight and better strength. The weight of chitosan-based self-powered sensing fiber with a length of 20 cm is only 0.023 g. It can also withstand a weight of 200 g without breaking, as can be seen in Fig. 2e, f. It also has the same fineness as ordinary sewing yarn to

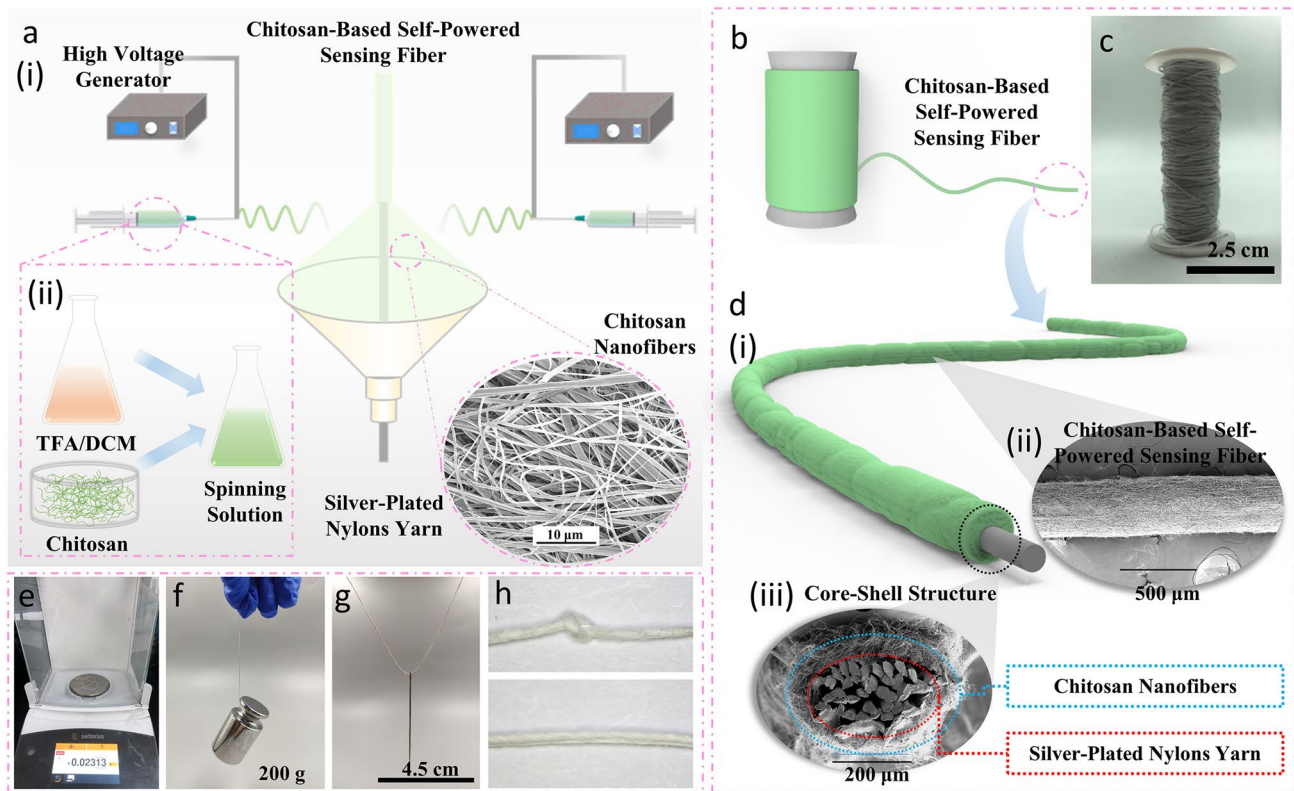


**Fig. 2** Preparation process and demonstration of chitosan-based self-powered sensing fiber. **a** The preparation process of chitosan-based self-powered sensing fiber. (i) Diagram of an electrospinning device. (ii) Preparation of chitosan electrospraying solution. **b** Schematic diagram of the bobbin of chitosan-based self-powered sensing fiber. **c** Physical picture of the bobbin of chitosan-based self-powered sensing fiber. **d** The structure diagram of chitosan-based self-powered sensing fiber. (i) Schematic diagram of the structure of chitosan-based self-

powered sensing fiber. (ii) SEM picture of chitosan-based self-powered sensing fiber. (iii) SEM of the cross-section of chitosan-based self-powered sensing fiber. **e** Picture of the weight of chitosan-based self-powered sensing fiber. **f** Physical picture of chitosan-based self-powered sensing fiber bearing 200 g. **g** Physical picture of chitosan-based self-powered sensing fiber threading needle. **h** Chitosan-based self-powered sensing fiber knotting before and after the physical picture

pass through textile needles, as shown in Fig. 2g. In addition, thanks to the continuous electrospinning technique, the obtained chitosan nanofiber shell material is firmly attached around the conductive yarn, which facilitates the production of a very soft and stable chitosan-based self-powered sensing fibers. As shown in Fig. 2h, the shell layer in the knotted-disassembled region remains intact and tightly wrapped around the conductive yarn.

The present work also discusses the chitosan-based self-powered sensing fibers with different chitosan concentrations as shown in Fig. 3a–c for 1.5 wt%, 2 wt% and 2.5 wt%, respectively. When the chitosan concentration is 1.5 wt%, the chitosan nanofibers have uneven coarseness and lumps bonded together and the thickness of chitosan-based self-powered sensing fiber is not uniform. The concentration of chitosan is 2 wt% and the morphology of chitosan nanofibers is good, but a small amount of lumps is still present. When the concentration of chitosan is 2.5 wt%, the coarseness of chitosan nanofibers is uniform and no bonding is observed, and the coarseness of chitosan-based self-powered sensing

fibers is relatively uniform. Next, the properties of chitosan-based self-powered sensing fibers with different chitosan concentrations are investigated from both mechanical and electrical aspects. From the stress–strain curves of chitosan-based self-powered sensing fibers in Fig. 3d, it can be seen that some small changes in the strength of chitosan-based self-generating sensing fibers occurred with the change in chitosan concentration. When the chitosan concentration is 1.5 wt%, 2 wt% and 2.5 wt%, the tensile strength at the break of chitosan-based self-powered sensing fiber is 74.3 MPa, 67 MPa and 79.2 MPa, respectively. The elongation at break of chitosan-based self-powered sensing fiber is 116%, 121% and 127% when the chitosan concentration is 1.5 wt%, 2 wt% and 2.5 wt%, respectively. In addition, the strength and flexibility of chitosan-based self-powered sensing fibers can be adjusted by changing different conductive yarns to make them suitable for different scenarios (Fig. S4).

Figure 3e briefly illustrates the working principle of chitosan-based self-powered sensing fiber. It is a single electrode mode that works on the coupling effect of contact

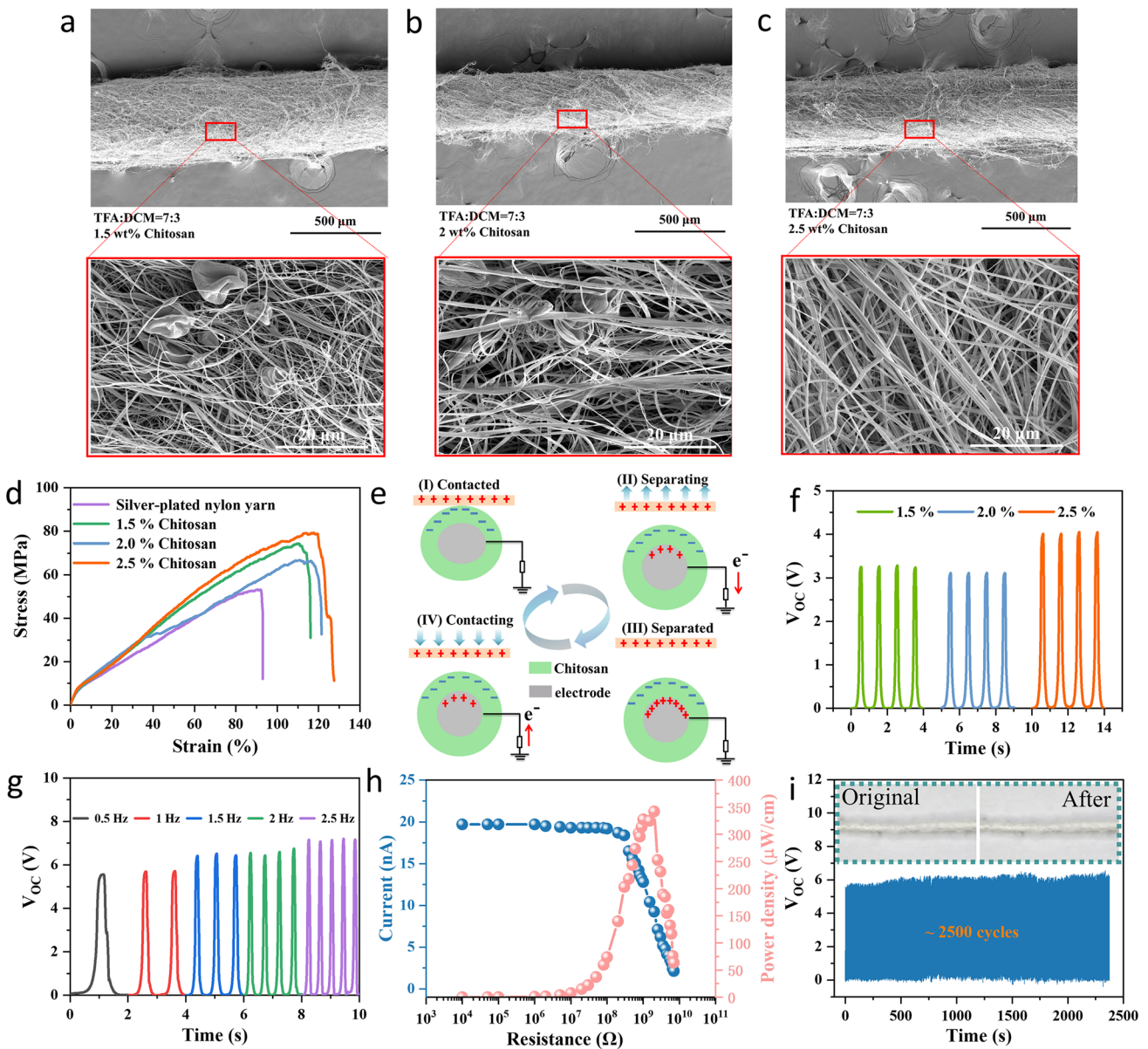


**Fig. 3** Performance of chitosan-based self-powered sensing fiber with different chitosan concentrations for a solvent TFA: DCM of 7:3. Surface morphology of chitosan-based self-powered sensing fiber with chitosan concentration of **a** 1.5 wt%, **b** 2 wt%, and **c** 2.5 wt%. **d** Stress–strain curves of chitosan-based self-powered sensing fiber with different chitosan concentrations. **e** Schematic diagram of the working principle of chitosan-based self-powered sensing fiber. **f**  $V_{OC}$  of chitosan-based self-powered sensing fiber with different chitosan

concentrations. **g**  $V_{OC}$  of chitosan-based self-powered sensing fiber at different frequencies with chitosan concentration of 2.5 wt%. **h** The variation of current and power density of chitosan-based self-powered sensing fiber with different external load resistance. **i** The stability test of the chitosan-based self-powered sensing fiber. The inset shows the situation of chitosan-based self-powered sensing fiber before and after the impact

electrification and electrostatic induction, which is achieved by periodic contact and separation movements between the fiber and its contact [1]. Taking human skin as the contact object, when the skin touches the fiber surface, the two contact surfaces generate equivalent positive and negative electrostatic charges, as shown in Fig. 3e(I). When the skin gradually moves away from the fiber surface, the potential

of the electrode layer will rise due to electrostatic induction, driving the flow of electrons to the ground, thus generating a current as shown in Fig. 3e(II). When the gap between the two charged surfaces is large enough, a new equilibrium state will be established and the electrons will stop moving as shown in Fig. 3e(III). When the skin approaches the fiber surface again, electrons will flow from the ground to the

electrode layer to reach a new charge equilibrium, as shown in Fig. 3e(IV). When the skin is in full contact with fiber again, the two surfaces are again in equilibrium. This is the entire working cycle of chitosan-based self-powered sensing fiber. Chitosan-based self-powered sensing fibers are tested for  $V_{OC}$  (Fig. 3f),  $I_{SC}$  (Fig. S5a) and  $Q_{SC}$  (Fig. S5b) with different chitosan concentrations at a contact pressure of 10 N for a length of 5 cm. At 1 Hz, the  $V_{OC}$  of chitosan-based self-powered sensing fiber with 1.5 wt% chitosan concentration is 3.23 V, the  $I_{SC}$  is 14.6 nA, and the  $Q_{SC}$  is 1.1 nC. The 2 wt% chitosan-based self-powered sensing fiber has a  $V_{OC}$  of 3.1 V, an  $I_{SC}$  of 15 nA, and a  $Q_{SC}$  of 1 nC. The 2.5 wt% chitosan-based self-powered sensing fiber has a  $V_{OC}$  of 4 V, an  $I_{SC}$  of 15 nA, and a  $Q_{SC}$  of 1.16 nC. In summary, the chitosan-based self-powered sensing fiber with 2.5 wt% chitosan concentration is selected for further investigation by combining the mechanical and electrical output properties.

The electrical output performance of chitosan-based self-powered sensing fibers (5 cm in length) is tested at different frequencies, as shown in Fig. 3g and Fig. S6a and b, with a chitosan concentration of 2.5 wt%. The  $V_{OC}$  and  $Q_{SC}$  of the fibers increase slightly with the increase of the impact frequency but basically stabilize to 6.4 V for  $V_{OC}$  and 1.26 nC for  $Q_{SC}$ , respectively, while the  $I_{SC}$  increases with the increase of the impact frequency, and the  $I_{SC}$  can reach 17.4 nA at a frequency of 2.5 Hz. Because the amount of charge generated by changing the frequency friction layer is constant at constant pressure (the amount of charge transferred between the two electrodes is also constant), the resulting open-circuit voltage also remains almost stable without large changes. And as the frequency increases, the rate of charge moving between the electrodes increases. As the rate of charge movement increases, the short-circuit current also increases. To obtain the maximum load power of the chitosan-based self-powered sensing fiber, the fiber is tested in series with different sizes of resistors, as shown in Fig. 3h. It can be seen that when the external resistance is small, the external circuit corresponds to a "short-circuit state" with almost no change. As the external load resistance increases, the current begins to decrease. At an external load resistance of 2 G $\Omega$ , the current is 9.29 nA, and the maximum power is 342  $\mu$ W cm $^{-1}$ . For wearable electronic devices, it is essential to maintain a certain level of stability, so this thesis also discusses the voltage output profile of the fiber after about 2,500 cycles of collisions, as shown in Fig. 3i. It can be seen that the output voltage of the fiber hardly changes significantly during the cycling process. In addition, it can be seen from the inset that after cyclic contact-separation, the surface of the fiber does not undergo major damage and still maintains a good core-yarn structure, indicating good stability of the fiber. The electrical energy generated by the chitosan-based self-powered sensing fiber can be stored in the capacitor to power electronic devices. Therefore, the

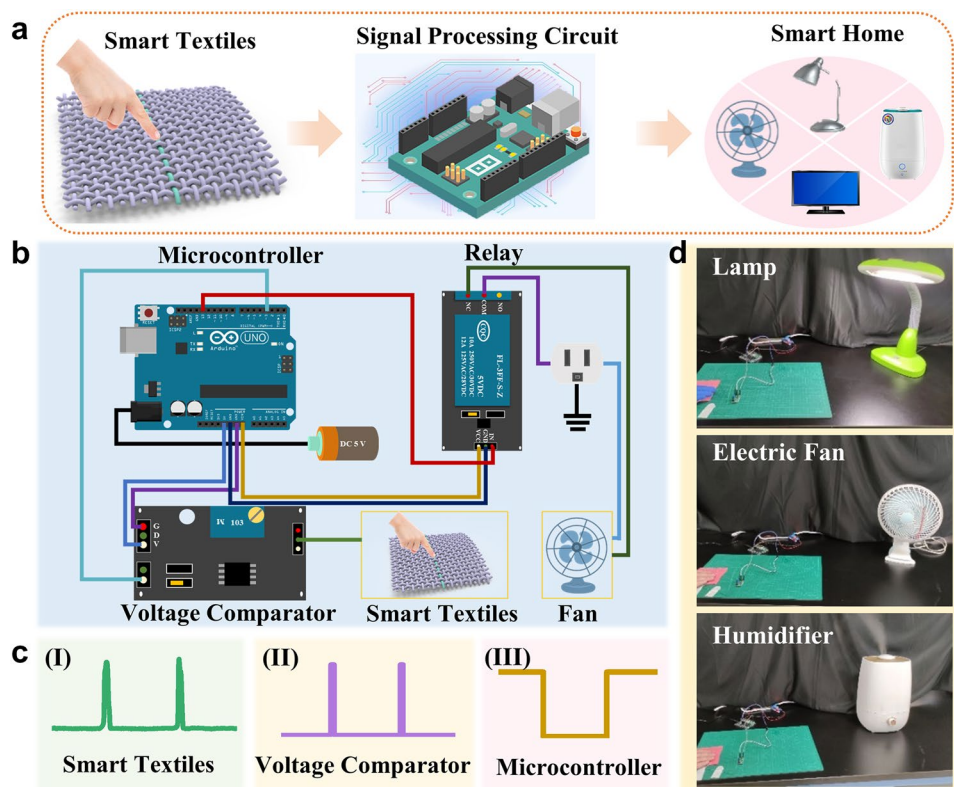
charging curve of chitosan-based self-powered sensing fiber with a length of 5 cm for different capacitance at 1 Hz is discussed, as shown in Fig. S7. It can be seen that the charging rate decreases as the capacitor capacity increases.

Since the chitosan-based self-powered sensing fiber can sense the fast contact-separation process in real time, it is applied to smart home control sensing for the smart home. As shown in Fig. 4a, this smart home control sensing circuit consists of chitosan-based self-powered sensing fiber, a signal processing circuit, and smart appliances. Figure 4b shows the circuit diagram of the smart home system, where the signal processing circuit includes a voltage comparator that converts the amplified signal into a stable square-wave signal (Fig. 4c(ii)). A microcontroller for receiving the square-wave signal and sending commands to relays to control high-power appliances. As shown in Fig. 4c(i), a voltage peak is generated when a contact separation occurs between the hand and the chitosan-based self-powered sensing fiber. When the voltage signal value is greater than the set threshold, the voltage comparator generates a "high potential" signal, as shown in Fig. 4c(ii). These signals are modulated by the microcontroller unit into a "low potential" or "high potential" command, and the "low potential" or "high potential" command is transmitted to the relay, as in Fig. 4c(iii). After receiving the command, the relay is set to "on" or "off", and the corresponding appliance will receive the signal to turn on or off. The command is set to turn on the appliance after the first contact separation between the hand and the chitosan-based self-powered sensing fiber. The actual transmission schematic of the smart home control sensing circuit is shown in Fig. S8. The applications of sensing fibers for the control of household appliances, including a table lamp, a monitor, a fan, and a humidifier, are shown separately in Fig. 4d and Fig. S9 (Supporting Movie S1). It indicates that there is a greater prospect of smart fiber in the field of smart homes.

## Conclusions

In this work, chitin is first extracted from waste materials (such as shrimp shells) by chemical treatment, and then chitosan is obtained by deacetylation of chitin. During the chemical treatment, the macroscopic morphology as well as the microscopic morphology of the shrimp shells are changed more clearly. The shrimp shells before and after the deacetylation reaction are characterized by XRD, FT-IR and TG, and it is found that chitin is converted to chitosan after deacetylation treatment. The chitosan-based self-powered sensing fibers by electrospinning technique, and the fiber has good flexibility. The mechanical properties of chitosan-based self-powered sensing fibers are similar to those of the conductive yarn in the center of the fiber, and the mechanical properties of the

**Fig. 4** Application of the chitosan-based self-powered sensing fiber in smart home control. **a** Schematic diagram of the smart appliance control system. **b** Schematic diagram of the circuit of the smart home appliance control system. **c** (i) Voltage signal generated by chitosan-based self-powered sensing fiber. (ii) The signal generated by the voltage comparator. (iii) The signal transmitted to the relay by the microcontroller. **d** Control different smart appliances



fiber can be controlled by adjusting or replacing the conductive yarn to achieve the performance requirements in different scenarios. In addition, chitosan-based self-powered sensing fibers can be integrated into clothing as a self-powered sensor, and this experiment has used the device as a smart switch sensor to control the start-up and shutdown of household appliances, which has a wide application prospect in the field of self-powered sensing.

**Supplementary Information** The online version contains supplementary material available at <https://doi.org/10.1007/s42765-022-00194-z>.

**Acknowledgements** The authors are grateful for the support received from National Natural Science Foundation of China (Grant No. 22109012), Natural Science Foundation of the Beijing Municipality (Grant No. 2212052), and the Fundamental Research Funds for the Central Universities (Grant No. E1E46805).

## Declarations

**Conflict of interest** The authors declare no conflict of interest.

## References

1. Dong K, Peng X, Cheng R, Ning C, Jiang Y, Zhang Y, Wang ZL. Advances in high-performance autonomous energy and self-powered sensing textiles with novel 3D fabric structures. *Adv Mater* 2022;34:e2109355.
2. Shi X, Luo J, Luo J, Li X, Han K, Li D, Cao X, Wang ZL. Flexible wood-based triboelectric self-powered smart home system. *ACS Nano* 2022;16:3341.
3. Yang Y, Xie L, Wen Z, Chen C, Chen X, Wei A, Cheng P, Xie X, Sun X. Coaxial triboelectric nanogenerator and supercapacitor fiber-based self-charging power fabric. *ACS Appl Mater Interfaces* 2018;10:42356.
4. Kim H, Shaqee A, Han S, Kang J, Yun J, Lee M, Lee S, Kim J, Noh S, Choi M, Lee J. In situ formation of Ag nanoparticles for fiber strain sensors: toward textile-based wearable applications. *ACS Appl Mater Interfaces* 2021;13:39868.
5. Wang H, Zhang Y, Liang X, Zhang Y. Smart fibers and textiles for personal health management. *ACS Nano* 2021;15:12497.
6. Roudjane M, Bellemare-Rousseau S, Drouin E, Belanger-Huot B, Dugas M-A, Miled A, Messadeq Y. Smart T-shirt based on wireless communication spiral fiber sensor array for real-time breath monitoring: validation of the technology. *IEEE Sens J* 2020;20:10841.
7. Ning C, Cheng R, Jiang Y, Sheng F, Yi J, Shen S, Zhang Y, Peng X, Dong K, Wang ZL. Helical fiber strain sensors based on triboelectric nanogenerators for self-powered human respiratory monitoring. *ACS Nano* 2022;16:2811.
8. Peng X, Dong K, Ning C, Cheng R, Yi J, Zhang Y, Sheng F, Wu Z, Wang ZL. All-nanofiber self-powered skin-interfaced real-time respiratory monitoring system for obstructive sleep apnea-hypopnea syndrome diagnosing. *Adv Funct Mater* 2021;31:2103559.
9. Wang R, Du Z, Xia Z, Liu J, Li P, Wu Z, Yue Y, Xiang Y, Meng J, Liu D, Xu W, Tao X, Tao G, Su B. Magnetoelectrical clothing generator for high-performance transduction from biomechanical energy to electricity. *Adv Funct Mater* 2021;32:2107682.
10. Wang D, Wang L, Shen G. Nanofiber/nanowires-based flexible and stretchable sensors. *J Semicond* 2020;41:041605.
11. Joyce BL, Harmon MJ, Johnson RGH, Hicks V, Brown-Schott N, Pilling LB. Using a quality improvement model to enhance

- community/public health nursing education. *Public Health Nurs* **2019**;36:847.
12. Dong K, Peng X, An J, Wang AC, Luo J, Sun B, Wang J, Wang ZL. Shape adaptable and highly resilient 3D braided triboelectric nanogenerators as e-textiles for power and sensing. *Nat Commun* **2020**;11:1.
  13. Wang ZL. Triboelectric nanogenerators as new energy technology and self-powered sensors-principles, problems and perspectives. *Faraday Discuss* **2014**;176:447.
  14. Wang ZL. On Maxwell's displacement current for energy and sensors: the origin of nanogenerators. *Mater Today* **2017**;20:74.
  15. Wang ZL, Chen J, Lin L. Progress in triboelectric nanogenerators as a new energy technology and self-powered sensors. *Energy Environ Sci* **2015**;8:2250.
  16. Shuai L, Guo ZH, Zhang P, Wan J, Pu X, Wang ZL. Stretchable, self-healing, conductive hydrogel fibers for strain sensing and triboelectric energy-harvesting smart textiles. *Nano Energy* **2020**;78:105389.
  17. Dong K, Wang Z. Self-charging power textiles integrating energy harvesting triboelectric nanogenerators with energy storage batteries/supercapacitors. *J Semicond* **2021**;38:105009.
  18. Dong K, Deng J, Zi Y, Wang YC, Xu C, Zou H, Ding W, Dai Y, Gu B, Sun B, Wang ZL. 3D orthogonal woven triboelectric nanogenerator for effective biomechanical energy harvesting and as self-powered active motion sensors. *Adv Mater* **2017**;29:1702648.
  19. Cheng R, Dong K, Chen P, Ning C, Peng X, Zhang Y, Liu D, Wang ZL. High output direct-current power fabrics based on the air breakdown effect. *Energy Environ Sci* **2021**;14:2460.
  20. Wang F, Ren Z, Nie J, Tian J, Ding Y, Chen X. Self-powered sensor based on bionic antennae arrays and triboelectric nanogenerator for identifying noncontact motions. *Adv Mater Technol* **2019**;5:1900789.
  21. Jiang Y, Zhang Y, Ning C, Ji Q, Peng X, Dong K, Wang ZL. Ultrathin eardrum-inspired self-powered acoustic sensor for vocal synchronization recognition with the assistance of machine learning. *Small* **2022**;18:e2106960.
  22. Ma L, Wu R, Patil A, Yi J, Liu D, Fan X, Sheng F, Zhang Y, Liu S, Shen S, Wang J, Wang ZL. Acid and alkali-resistant textile triboelectric nanogenerator as a smart protective suit for liquid energy harvesting and self-powered monitoring in high-risk environments. *Adv Funct Mater* **2021**;31:2102963.
  23. Jin L, Zhang B, Zhang L, Yang W. Nanogenerator as new energy technology for self-powered intelligent transportation system. *Nano Energy* **2019**;66:104086.
  24. Chen H, Lu Q, Cao X, Wang N, Wang ZL. Natural polymers based triboelectric nanogenerator for harvesting biomechanical energy and monitoring human motion. *Nano Res* **2021**;15:2505.
  25. Dong K, Peng X, Cheng R, Wang ZL. Smart textile triboelectric nanogenerators: prospective strategies for improving electricity output performance. *Nanoenergy Adv* **2022**;2:133.
  26. Zhao Z, Zhou L, Li S, Liu D, Li Y, Gao Y, Liu Y, Dai Y, Wang J, Wang ZL. Selection rules of triboelectric materials for direct-current triboelectric nanogenerator. *Nat Commun* **2021**;12:1.
  27. Chen Y, Zhang Q, Zhong Y, Wei P, Yu X, Huang J, Cai J. Super-strong and super-stiff chitosan filaments with highly ordered hierarchical structure. *Adv Funct Mater* **2021**;31:2104368.
  28. Guibal E. Heterogeneous catalysis on chitosan-based materials: a review. *Prog Polym Sci* **2005**;30:71.
  29. Crini G, Badot P-M. Application of chitosan, a natural aminopolysaccharide, for dye removal from aqueous solutions by adsorption processes using batch studies: a review of recent literature. *Prog Polym Sci* **2008**;33:399.
  30. Morin-Crini N, Lichtfouse E, Torri G, Crini G. Applications of chitosan in food, pharmaceuticals, medicine, cosmetics, agriculture, textiles, pulp and paper, biotechnology, and environmental chemistry. *Environ Chem Lett* **2019**;17:1667.
  31. Pillai CKS, Paul W, Sharma CP. Chitin and chitosan polymers: chemistry, solubility and fiber formation. *Prog Polym Sci* **2009**;34:641.
  32. Peng X, Dong K, Zhang Y, Wang L, Wei C, Lv T, Wang ZL, Wu Z. Sweat-permeable, biodegradable, transparent and self-powered chitosan-based electronic skin with ultrathin elastic gold nanofibers. *Adv Funct Mater* **2022**;32:2112241.
  33. Kim J-N, Lee J, Go TW, Rajabi-Abhari A, Mahato M, Park JY, Lee H, Oh I-K. Skin-attachable and biofriendly chitosan-diatom triboelectric nanogenerator. *Nano Energy* **2020**;75:104904.
  34. Xu Z, Zhang D, Liu X, Yang Y, Wang X, Xue Q. Self-powered multifunctional monitoring and analysis system based on dual-trioboelectric nanogenerator and chitosan/activated carbon film humidity sensor. *Nano Energy* **2022**;94:106881.
  35. Ohkawa K, Cha D, Kim H, Nishida A, Yamamoto H. Electrospinning of chitosan. *Macromol Rapid Commun* **2004**;25:1600.
  36. Jacobs V, Patanaik A, Anandjiwala RD, Maaza M. Optimization of electrospinning parameters for chitosan nanofibres. *Curr Nanosci* **2011**;7:396.
  37. Sangsanoh P, Supaphol P. Stability improvement of electrospun chitosan nanofibrous membranes in neutral or weak basic aqueous solutions. *Biomacromol* **2006**;7:2710.

**Publisher's Note** Springer Nature remains neutral with regard to jurisdictional claims in published maps and institutional affiliations.

Springer Nature or its licensor holds exclusive rights to this article under a publishing agreement with the author(s) or other rightsholder(s); author self-archiving of the accepted manuscript version of this article is solely governed by the terms of such publishing agreement and applicable law.



**Yingying Li** received her B.S. degree from Luoyang Normal University in 2018 and her M.S. degree from Guangxi University in 2022. She is jointly cultivated in Beijing Institute of Nanoenergy and Nanosystems, Chinese Academy of Sciences from 2020 to 2022. Her main research direction is wearable fiber and self-powered sensor system based on triboelectric nano generator.



**Chuanhui Wei** received his B.S. degree from Qingdao University of Science and Technology in 2020. Now he is pursuing his M.S. degree in Beijing Institute of Nanoenergy and Nanosystems, Chinese Academy of Sciences. His research interests are mainly focused on multifunctional wearable electronics and self-powered sensor systems based on triboelectric nanogenerator.



**Yang Jiang** received her Ph.D. in Material Sciences from Beijing Institute of Nanoenergy and Nanosystems, Chinese Academy of Sciences. Her research interests are mainly focused on the self-powered wearable electronics for mechanical energy harvesting and pressure/physiological signals sensing based on triboelectric nanogenerators.



**Renwei Cheng** received his B.S. degree in Electronic Science and Technology from University of Electronic Science and Technology of China in 2018. Now he is pursuing his Ph.D. degree in Beijing Institute of Nanoenergy and Nanosystems, Chinese Academy of Sciences. His research interests are mainly focused on wearable energy harvesting and self-powered sensors based on triboelectric nanogenerator.



**Yihan Zhang** is now studying for his Ph.D. at the University of Sussex, UK. He obtained his master degree from the University of the Chinese Academy of Sciences in 2022 and his Bachelor of engineering degree from Zhengzhou University in 2019.



**Chuan Ning** received his M.S. degree from Zhengzhou University in 2019. He received his Ph.D. degree from Beijing Institute of Nanoenergy and Nanosystems, Chinese Academy of Sciences in 2022. Currently, he is a teacher at the College of Materials Science and Engineering, Zhengzhou University. His research interests include smart/electronic textiles, fiber/fabric-based triboelectric nanogenerators and self-powered wearable sensors.



**Kai Dong** is an associate professor at the Beijing Institute of Nanoenergy and Nanosystems, Chinese Academy of Sciences. He received his M.S. and Ph.D. degrees in textile science and engineering from Donghua University in 2015 and 2018, respectively. He joined Donghua University from November 2018 to June 2019 as a faculty member. He was a visiting scholar of Georgia Institute of Technology from 2016 to 2018. His research interests include high-performance autonomous energy and

self-powered sensing textiles based on triboelectric and piezoelectric effects, smart/electronic textiles, flexible electronics, electronic skins, and so on. He has published more than 60 articles, including *Nat. Commun.*, *Sci. Adv.*, *Adv. Mater.*, *Energy Environ. Sci.*, *Adv. Energy Mater.*, *ACS Nano*, and so on.



**Zhong Lin Wang** Wang is the Hightower Chair in Materials Science and Engineering and Regents' Professor at Georgia Tech, and Founding Director and Chief Scientist at Beijing Institute of Nanoenergy and Nanosystems, Chinese Academy of Sciences. He pioneered nanogenerators from fundamental principles to technological applications. He coined and pioneered the fields of piezotronics and piezo-phototronics for third-generation semiconductors. His research on self-powered nanosystems has inspired the worldwide effort within academia and industry to study energy for micro–nano-systems, which is now a distinct discipline in energy research and future sensor networks.